JACS
JOURNAL OF THE AMERICAN CHEMICAL SOCIETY
Article
pubs.acs.org/JACS

# Electrochemical Activation of Cp* Iridium Complexes for Electrode-Driven Water-Oxidation Catalysis

Julianne M. Thomsen,[†] Stafford W. Sheehan,[†] Sara M. Hashmi,[‡] Jesús Campos,[†] Ulrich Hintermair,*[,†,§] Robert H. Crabtree,[†] and Gary W. Brudvig*[,†]

[†]Department of Chemistry, Yale University, 225 Prospect Street, New Haven, Connecticut 06520, United States

[‡]Department of Chemical and Environmental Engineering, Yale University, 9 Hillhouse Avenue, New Haven, Connecticut 06520, United States

[§]Centre for Sustainable Chemical Technologies, University of Bath, Bath BA2 7AY, United Kingdom

Supporting Information

**ABSTRACT:** Organometallic iridium complexes bearing oxidatively stable chelate ligands are precursors for efficient homogeneous water-oxidation catalysts (WOCs), but their activity in oxygen evolution has so far been studied almost exclusively with sacrificial chemical oxidants. In this report, we study the electrochemical activation of Cp*Ir complexes and demonstrate true electrode-driven water oxidation catalyzed by a homogeneous iridium species in solution. Whereas the Cp* precursors exhibit no measurable $O_2$-evolution activity, the molecular species formed after their oxidative activation are highly active homogeneous WOCs, capable of electrode-driven $O_2$ evolution with high Faradaic efficiency. We have ruled out the formation of heterogeneous iridium oxides, either as colloids in solution or as deposits on the surface of the electrode, and found indication that the conversion of the precursor to the active molecular species occurs by a similar process whether carried out by chemical or electrochemical methods. This work makes these WOCs more practical for application in photoelectrochemical dyads for light-driven water splitting.

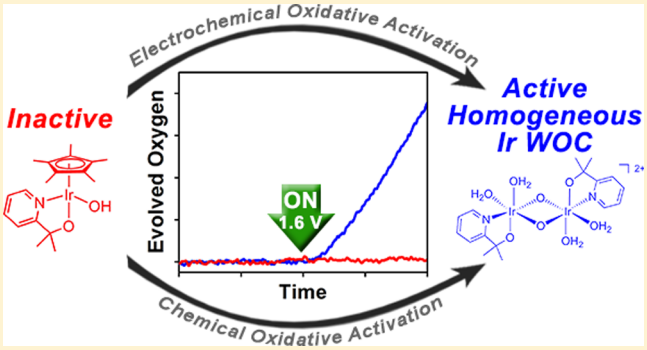


## INTRODUCTION

With global energy demand rising, the need for sustainable and non-polluting energy sources is becoming increasingly urgent.[1] Artificial photosynthesis is a promising strategy for meeting growing energy demands, borrowing a time-tested scheme from nature for the storage of energy from sunlight in the chemical bonds of fuels.[2−4] The crucial half-reaction in both natural and artificial photosynthesis is water oxidation, in which solar energy is used to split two molecules of water into molecular oxygen, electrons, and protons. The protons and electrons harvested from water in this manner can then be used for the formation of sustainable energy carriers and chemical feedstocks.[5] Water oxidation is an endergonic four-electron process with a standard reduction potential of 1.23 V, which in practice, however, requires large additional overpotentials to drive the kinetics. To ease these energetic demands, effective catalysts are needed to make this reaction as efficient as possible. Thus, identifying robust water-oxidation catalysts (WOCs) with low overpotentials and high activities has been an active area of research.[6−8]

The number of catalyst candidates for water oxidation has grown substantially in the past 10 years.[6,8,9] Among these are the family of Cp*Ir precatalysts introduced by our group in 2009,[10] of which three archetypical members are shown in Chart 1. Solutions initially containing these species were shown to evolve oxygen from water with the addition of an excess of cerium(IV) ammonium nitrate (CAN) or sodium periodate ($NaIO_4$) as sacrificial chemical oxidant. A subsequent report[11] showed the electrochemical behavior of these Cp*Ir complexes in aqueous solution to be consistent with water-oxidation catalysis, though there was no definitive assignment by correlation of current with oxygen evolution.

**Chart 1. Previously Reported Iridium Precatalysts for Catalytic Oxygen Evolution from Water**

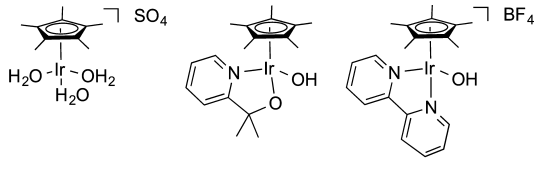


1 2 3

Subsequent reports from our groups[12,13] and others[14] noted the rapid formation of characteristic absorption maxima in the

Received: July 11, 2014
Published: September 4, 2014

   dx.doi.org/10.1021/ja5068299 | J. Am. Chem. Soc. 2014, 136, 13826−13834

range of 570−610 nm in the UV−visible spectra upon the addition of chemical oxidants to Cp*Ir complexes, giving these solutions an intense blue color. Macchioni and co-workers carried out detailed NMR studies of these compounds upon addition of CAN as well as $H_2O_2$, finding degradation of Cp* to acetic, formic, and glycolic acids,[15,16] and others have reported similar findings.[17−19] Our kinetic experiments have shown that the formation of this blue species correlates with the oxidative removal of the Cp* ligand and onset of $O_2$-evolution activity,[20] suggesting that the Cp*Ir complexes are catalyst precursors and the blue species are the true active catalysts. Since hydrated iridium(IV) oxides are often blue-colored,[21−26] multiple groups suggested that the blue species generated by chemical oxidation of Cp*Ir complexes could be explained as total degradation of the molecular complexes and polymerization into heterogeneous iridium oxide materials.[14,27] Transmission electron microscopy (TEM) was most often used to characterize the nanoparticles that were thought to have been formed in the reaction medium. However, the TEM sample preparation procedures and the heating and reducing conditions caused by the high-energy electron beam in a TEM may induce particle and cluster formation in initially particle-free samples.[28] We have, therefore, employed a number of other methods to look for evidence of complex degradation during turnover in solution (*in operando*).[13,28−30] We performed time-resolved electrochemical quartz-crystal nanobalance (EQCN) experiments to look for deposition of heterogeneous material during electrochemical oxidation of Cp*Ir complexes,[29] finding that complex **1**, which had been observed to leave blue deposits on electrodes with potential cycling, deposited mass on electrode surfaces when an oxidizing potential was applied. However, the trifluoroacetate analog of complex **2** and the sulfate analog of complex **3**[31] did not yield any such mass deposition, suggesting homogeneous catalysis when the 2-(2′-pyridyl)-2-propanoate (pyalc) ligand was present in the precursor. A subsequent study used time-resolved dynamic light scattering (DLS) to monitor particle formation during chemical oxidation in solutions confirmed that, while complex **1** gave rise to intense scattering characteristic of particle formation within minutes of $NaIO_4$ addition, complexes **2** and **3** did not show any scattering, even many hours after oxidation with a large excess of oxidant.[13] This study also showed that changing the concentrations of both oxidant and complex significantly affected the size distribution and rate of formation of particles, as did changing the pH and the presence of soluble salts in the medium, all factors that could complicate the interpretation of findings on similar systems.[14,27]

Recent detailed studies of the homogeneous blue solution formed from $NaIO_4$ and the Cp*Ir complex **2** gave more insights into precursor transformation and confirmed the molecular nature of the blue species.[20] A number of characterization methods, including MALDI-TOF mass spectrometry, X-ray photoelectron spectroscopy (XPS), $^{17}O$ NMR spectroscopy, and resonance Raman spectroscopy in conjunction with time-dependent density functional theory modeling, ultimately suggested the active blue species to be a di-$\mu$-oxo iridium(IV,IV) dimer comprising one chelate ligand and two bound waters per iridium center (Scheme 1, complex **4**). Importantly, these findings were fully compatible with all previously reported data and observations regardless of their interpretation, including chelate ligand effects on the $\lambda_{max}$ of the resulting blue solutions and the fact that $(cod)Ir^{I}$ complexes

**Scheme 1. Reaction of 2 with Excess Sodium Periodate in Aqueous Solution Results in an Activated Blue Species, with the Proposed[20] Structure Shown (4)**

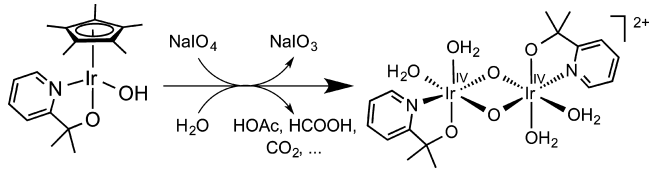


**2** **4**

with the same chelate gave results nearly identical to those obtained with the analogous $Cp^*Ir^{III}$ precursors.[20]

In photoelectrochemical solar fuel applications, the active catalytic species must be driven in one-electron steps.[32] Use of $NaIO_4$ to drive catalysis is rather inconclusive as to a catalyst's suitability for photoelectrochemical application, as $IO_4^-$ can act as a two-electron oxidant.[33] Additionally, non-innocent electron-transfer pathways have been hypothesized for other chemical oxidants, such as CAN.[34,35] Complications such as these, in addition to fundamental differences in their charge-transfer reactions, cause chemical oxidants to be rather poor electrode surrogates. These points mean that any promising candidate precatalyst must be examined for electrocatalytic activity once it has been demonstrated to be useful by chemical oxidation. However, this aspect is not often conclusively investigated because these experiments can be more challenging than equivalent trials using chemical oxidants. The time scale of electrochemical water oxidation is typically much slower than that when chemical oxidants are used due to the physical limitations imposed by mass transport, electrode surface area, and cell geometry.[36] Solution-phase electrocatalysis at electrodes with small surface areas thus necessarily results in low oxygen yields, making accurate, real-time measurement of $O_2$ evolution difficult. Typically, electrochemical cells must be custom-made in order to couple time-resolved oxygen measurements with electrolysis, and leakage of atmospheric oxygen can cause erroneously high oxygen yields. As a consequence of the logistical challenges of this type of experiment, there are very few reports in the literature of time-correlated measurement of $O_2$ evolution of solution-phase WOCs driven by electrodes.[37,38]

In this report, we investigate the electrochemical activation of **2** and quantify the electrocatalytic $O_2$-evolution performance of its activated molecular species by a Clark electrode setup able to detect sub-micromolar changes in $O_2$ concentration in the liquid phase at high temporal resolution. Significantly, no measurable oxygen is evolved from the precursor complex **2** at the potentials studied. Bulk electrolysis of the precursor species, however, yields a blue solution that is electrocatalytically active for water oxidation, as is the chemically activated analogue. DLS experiments and electron microscopy show no evidence of heterogeneous particles or films for either process. Although it also gives a homogeneous system after oxidative activation, clear differences in electrochemical and electrocatalytic behaviors are evident when **3** is used as the precursor rather than **2**, whether chemical or electrochemical activation is used, demonstrating that the choice of chelate ligand is important in determining the properties of the active catalyst. Altogether, the observations suggest that both methods of activation yield well-defined molecular species retaining the original chelate ligand,


dx.doi.org/10.1021/ja5068299 | J. Am. Chem. Soc. 2014, 136, 13826−13834

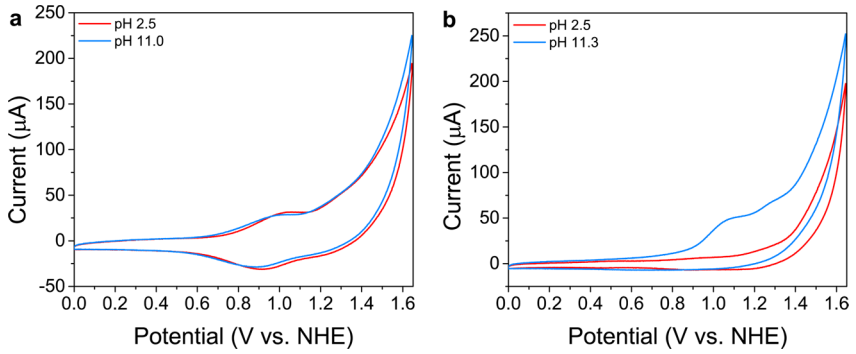


**Figure 1.** Cyclic voltammograms of (a) 1 mM **2** and (b) 1 mM **3** in acidic and basic pH regimes (conditions: 0.1 M $KNO_3$ supporting electrolyte pH adjusted with KOH or $HNO_3$, basal plane graphite working electrode, Ag/AgCl reference electrode, 500 mV/s scan rate).

and that the activated molecular species are likely similar, regardless of which method is used for activation.

## RESULTS AND DISCUSSION

In light of our recent findings on activation of Cp*Ir precatalysts with $NaIO_4$ showing that the Cp* ligand is degraded,[20] we carefully re-investigated the electrochemical behavior of complexes **2** and **3** to assess their water-oxidation activity. If water oxidation was directly accessible as the dominant electrochemical process, it would be expected to show a strong pH dependence, with a more basic solution giving rise to an earlier onset of catalytic current or greater current at higher pH,[39] as we have seen before for complex **3**.[11] Cyclic voltammograms (CVs) of aqueous solutions of **2** and **3**, however, showed surprisingly different behaviors in acidic and basic regimes (Figure 1 and Supporting Information Figures S1 and S2). Under acidic conditions, complex **2** (Figure 1a) had a broad, strongly scan-rate-dependent couple (Figure S1a,b) centered at 0.95 V vs NHE, which we assign to Ir(III)/Ir(IV), and the onset of a strong irreversible wave at 1.20 V. Under basic conditions, the Ir(III)/Ir(IV) couple shifted slightly to ca. 0.85 V, with a similar scan-rate dependence (Figure S1c,d). Surprisingly, however, the potential at which the irreversible wave began to appear did not shift substantially at elevated pH as expected for catalytic water oxidation; neither did the current at the highest applied voltage (1.65 V) substantially increase at elevated pH. This was in stark contrast to **3**, which showed significantly different behavior in the two regimes (Figure 1b, Figure S2). The onset of the irreversible wave shifted by approximately 60 mV/pH unit for **3**; however, this irreversible wave did not appear until pH 7.5 (Figure S3). Because bipyridine ligand oxidation has been reported for metal complexes above pH 7,[40−42] and this process is known to be pH-dependent, we now ascribe these features of the CV of **3** to bipyridine oxidation rather than water oxidation. The oxidation observed for **3** under basic conditions is interesting in light of the significant body of work performed on Cp*Ir bipyridine complexes.[14,17,27,43,44] The irreversible ligand-oxidation process has been described[40,45] as $OH^-$ attack on the bipyridine ring to form a dearomatized radical, followed by oxidative hydroxylation of the ring. Hydroxyl substituents render the bipyridine ring easier to oxidize further, ultimately leading to complete ligand degradation. Consistent with this observation, Cp*Ir complexes containing hydroxo-substituted bipyridine ligands have been seen to degrade to $IrO_x$ when used with CAN.[27] Importantly, however, this electrochemical behavior suggests that the oxidative features observed for both **2** and **3** by CV do not reflect catalytic water oxidation.

We then measured the $O_2$-evolution activity of the precursor **2** compared with its activated blue species **4** generated by prior activation with an excess of $NaIO_4$. Oxygen levels in the liquid phase were quantified by a highly sensitive Clark electrode while stepping the potential up to 1.6 V, which we predicted to be sufficiently high to drive $O_2$ evolution based on the known reduction potential of $NaIO_4$ (estimated between 1.5 and 1.6 V vs NHE at pH 2.5) that does lead to $O_2$ evolution in the absence of an electrode.[12,46] For these studies, a gold electrode was used, because carbon electrodes are prone to oxidative damage at the high potentials and longer durations required for these experiments. This damage is accelerated by iridium. CVs of iridium complexes with gold did not show significant differences from those collected using carbon electrodes (Figures S1 and S2). The electrolyte utilized for these experiments was the $NaIO_3$ that remained in solution after activation of complex **2**;[20] to control for any electrolyte-related effects, the supporting electrolyte used for the precursor **2** was also $IO_3^-$-based. Pre-activation of **2** with 100 equiv of $NaIO_4$ (0.10 M) caused baseline $O_2$ levels to be significantly higher than dissolved atmospheric $O_2$, so before the $O_2$-evolution measurements, pre-activated blue species **4** was purged with $N_2$ to drive off the $O_2$ evolved during the activation process and then stirred in air to achieve ambient levels of dissolved $O_2$. The potential was then held at 0 V vs NHE for a 10 min period while baseline $O_2$ levels were measured, followed by a potential step to 1.6 V, well past the onset of the irreversible wave of **2**. As shown in Figure 2, no $O_2$ was detected from **2** nor from the control experiment of $KIO_3$ with no iridium present at this potential, agreeing with the hypothesis that the oxidative features seen in the aqueous CVs of the Cp* complexes do not represent water oxidation. By contrast, pre-activated **4** evolved significant amounts of $O_2$ without a significant lag phase and a Faradaic efficiency of 59% (±5%) under identical conditions.

It is difficult to calculate a catalyst turnover rate directly from this measurement, because catalysis only occurs within the small reaction layer at the surface of the electrode and, therefore, only by a very small percentage of the total iridium in solution.[47] Thus, to provide comparable activity metrics, evolved $O_2$ is reported per iridium concentration per electrode surface area (0.017 $cm^2$). The measured rate of $O_2$ evolution at pH 2.1 for activated **4** was 8.5 (±0.5) nmol $O_2$ mM $Ir^{-1}$ $cm^{-2}$ $s^{-1}$, allowing for comparison of relative rates of $O_2$ evolution from different catalysts and reaction conditions.


dx.doi.org/10.1021/ja5068299 | J. Am. Chem. Soc. 2014, 136, 13826−13834

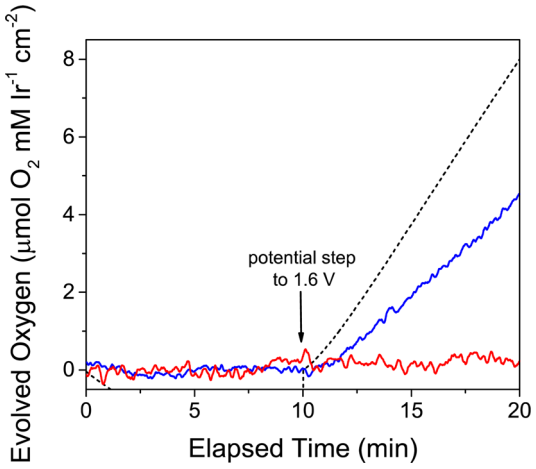


**Figure 2.** $O_2$ evolution over time in response to applied potential at a gold electrode. The electrode was held at 0 V vs NHE for the first 10 min, followed by a step to 1.60 V vs NHE for the second 10 min. Red, 1 mM **2** in 0.1 M $KIO_3$; blue, 1.2 mM **4** pre-activated with 100 equiv of $NaIO_4$; dashed black, predicted $O_2$ from current passed from pre-activated **4**).

Further experiments revealed that $O_2$ evolution became measurable using our apparatus at an applied potential of 1.45 V vs NHE, corresponding to an overpotential of 385 mV at pH 2.75. In this context, *overpotential* is defined as the potential at which $O_2$ evolution is detected via Clark electrode rather than the potential required to achieve a set current density (in our past work, 0.5 mA/cm$^2$),[48−50] which is only appropriate for surface-bound catalytic species.[36,51] This is among the lowest overpotentials observed for homogeneous WOCs,[37,38,52] although Meyer and co-workers have recently reported base-assisted water-oxidation catalysis with an exceedingly low overpotential of 180 mV.[53] Importantly, we have been able to correlate the current passed in our electrochemical experiments in real time with the concomitant formation of $O_2$ as product. The striking differences between the activated complex **4** and its precursor species **2** highlight the importance of this correlation, with both species showing above-background current but only **4** evolving $O_2$.

To ensure that the catalytic activity seen with activated **4** did not arise from iridium oxide deposits formed on the electrode surface during electrolysis (similar to those we have observed from other Cp*Ir precursors such as **1**[29,48]), the electrode was rinsed with deionized water, then placed in a solution of 0.25 M $KIO_3$ at pH 2.6 and the electrolysis experiment was repeated while monitoring $O_2$ evolution. This experiment showed negligible levels of current and $O_2$ evolution, suggesting no active material had deposited on the electrode surface during electrolysis (Figure S9). We also performed post-electrolysis scanning electron microscopy (SEM) and elemental analysis using energy-dispersive X-ray spectroscopy (EDX) of the unpolished electrodes. Again, no deposits of iridium and no coordination of the active catalyst were observed on the surface, with either gold or platinum as the working electrode (Figures S10 and S11). Use of $D_2O$ rather than $H_2O$ as the solvent during synthesis and then carrying out the electrochemical $O_2$-evolution experiment revealed a kinetic isotope effect (KIE) of 2.06 by comparing effective rates (Figure S24), which is very distinct from the KIE observed for heterogeneous iridium oxide species (usually no greater than 1.0−1.1).[54,55]

The Faradaic efficiency of only 59% indicates that water oxidation is not the only process occurring at the electrode surface. In $O_2$-evolution experiments on **4** formed by $NaIO_4$ pre-activation, residual $IO_4^-$-derived species remain in solution and we were concerned about their possible involvement. It is probable that reduced iodine species such as $I_2$ are formed by reaction of Cp* partial-oxidation products (such as formic acid or methanol) with $IO_3^-$ at acidic pH, and these iodine species are oxidized at lower potentials than water.[56] Such competing processes at the electrode could then result in lower Faradaic efficiency. Another concerning possibility is direct involvement of $IO_3^-$ as a redox mediator for $O_2$ evolution. As the standard reduction potential of $IO_4^-$ lies close to the potential at which the electrolysis was carried out,[46] it is possible that current passed during electrocatalytic $O_2$ evolution could arise from iridium-catalyzed oxidation of $IO_3^-$ to $IO_4^-$. The regenerated $IO_4^-$ could then react with nearby iridium catalysts to evolve oxygen, so that the overall process would be iodate-mediated water oxidation rather than genuine electrochemical water oxidation by iridium. The active involvement of periodate in $O_2$ evolution via its dismutation has been discussed[33] but is hard to track experimentally by isotope labeling because of its rapid oxygen exchange in aqueous solution.[12,46,57] Lastly, we were concerned that the chemical oxidants may be directly involved in the formation of the active species,[58] such as by oxygen-atom transfer from $IO_4^-$ to the precursor.[59]

To address these concerns, we attempted bulk electrolysis of **2** to see if it was possible to bypass the use of a chemical oxidant as activator and carry out an electro-oxidation to directly access the activated species **4**. Bulk electrolysis of a stirred aqueous solution of **2** at oxidizing potentials ($E_{app} \geq 1.4$ V vs NHE) with a high surface area platinum gauze electrode was carried out for extended periods of time. Owing to background currents arising from water oxidation by the platinum electrode, electrolyses were carried out under acidic conditions (pH 2.3−2.8) to reduce current overloads. Intriguingly, the familiar blue color began to develop in the solution shortly after initiation of electrolysis. Experiments varying the applied potential and duration of electrolysis ultimately led to a standard protocol of 36-h electrolysis of 1−1.25 mM Ir at 1.45 V in order to achieve full conversion of the precursor **2** to the blue species (see Supporting Information for complete details). Figure 3a shows UV−visible spectra of **2** before and after electrochemical activation, which exhibit a broad absorption around 600 nm reminiscent of **4** formed after chemical activation (Figure 3b). As in the case of activation by chemical oxidants, the $^1$H NMR spectrum of this electrogenerated blue solution showed the presence of acetic and formic acids from the oxidative degradation of the Cp* ligand (Figure S16). No Cp* resonances were present in the spectrum following bulk electrolysis. Direct comparison of the UV−visible spectra of this electrosynthesized species and chemically synthesized **4** shows some slight differences; certain features are absent in the spectrum of the electrogenerated species, most notably the shoulder at 450 nm. We suspected this absorption to be due to aqueous $I_2$ impurities from activation by $NaIO_4$ in the case of **4**, as $I_2$ has a substantial absorption in this range.[60] Addition of small amounts of $I_2$ to a solution of **2** after bulk electrolysis causes this peak to appear, confirming our suspicion (Figure S15). This control experiment also lends support to the notion that the low Faradaic efficiency of **4** is due to competitive $I_2$ oxidation.


dx.doi.org/10.1021/ja5068299 | J. Am. Chem. Soc. 2014, 136, 13826−13834

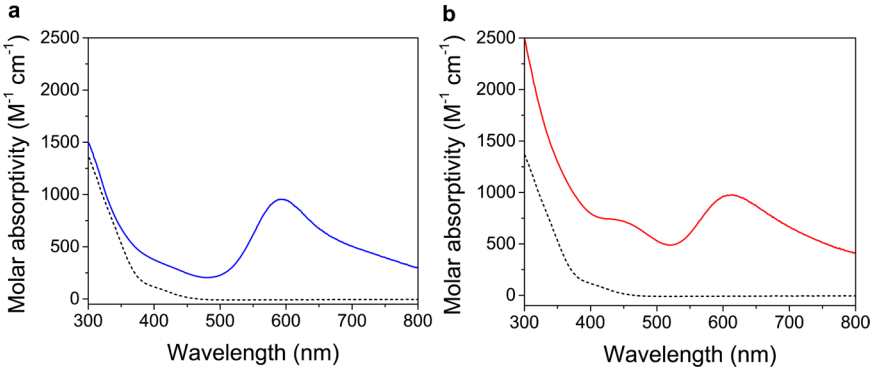


**Figure 3.** (a) UV−visible spectra of **2** before (dashed black) and after (solid blue) 36 h of electrolysis at a platinum electrode held at 1.45 V vs NHE in 0.25 M $Na_2SO_4$ electrolyte at pH 2.6. (b) UV−visible spectra of **2** before (dashed black) and 24 h after (solid red) treatment with 100 equiv of $NaIO_4$.

Since electrolysis has not only been used for the synthesis of iridium oxide films on electrode surfaces but also for making small $IrO_x$ nanoparticles in solution,[61] we examined the electrosynthesized blue solution by DLS as well as by TEM on dried samples. These data were both gathered for electrolyzed **2** as well as for reference samples of colloidal iridium oxide solutions synthesized following literature procedures.[21,25,26] As the iridium concentration is known to have a strong impact on nanoparticle formation,[13] the synthesis was done at 2.5 mM Ir and diluted to 1.25 mM Ir to compare to the sample prepared by bulk electrolysis (1.25 mM Ir). For comparison with previous studies, the standard activation procedure of **2** using 100 equiv of $NaIO_4$ to yield **4** was also used to make reference DLS samples (again at 2.4 and 1.2 mM Ir). The sample prepared by electrolysis was essentially indistinguishable from background $Na_2SO_4$ by DLS, while a discrete correlation function could be fit to the colloid synthesis (Figure S25). Ultrafiltration experiments carried out in tandem with DLS by Fujita and co-workers[62] have suggested that very small particles ($0.5 < x < 2$ nm) that can be trapped by filtration might have escaped detection by DLS and, therefore, the DLS measurement may have been inconclusive.[63] Significantly, however, repeated TEM experiments confirmed the lack of particles for electrolyzed **2** at both 2.3 mM and 1.3 mM while revealing very small clusters (∼2 nm) in the colloidal solutions synthesized by standard protocols (Figure 4, Figure S12). Thus, electrolytic activation of Cp*Ir precursors with robust chelate ligands may lead to similar molecular species as obtained when chemical oxidants are used. This finding suggests that the CV features above 1.2 V seen for these complexes reflect incipient precursor activation by Cp* oxidation, which agrees well with the absence of $O_2$ evolution and the indifference to pH variation (cf. Figure 1). As the fully activated samples exhibit greater current flow at 1.4 V (Figure S13), we further conclude that the initial steps of activating C−H oxidation must be slower than subsequent water oxidation in the fully activated state.

To further compare the blue species formed by electro-oxidation of **2** to that formed by chemical oxidation, the activity of the electrolyzed solution was examined for electrocatalytic water oxidation. As previously seen with pre-synthesized **4**, $O_2$ evolution occurred almost immediately, but this time with very high Faradaic efficiency (95% ± 5%) at 1.6 V (Figure 5). In the absence of iodine-based electrolytes, the effective rate of $O_2$ evolution from the electrosynthesized species also rose to 23 (±0.5) nmol $O_2$ mM $Ir^{-1}$ $cm^{-2}$ $s^{-1}$. To the best of our knowledge this is the highest rate reported for electrode-driven $O_2$ evolution by a solution-phase WOC. At the ambient pH of the solution after electrolysis (pH 1.8−2.3 due to proton production from concomitant water oxidation), $O_2$ evolution could be seen from applied potentials ≥1.45 V, or about 345 mV overpotential at pH 2 (Figure S21). In this case, the

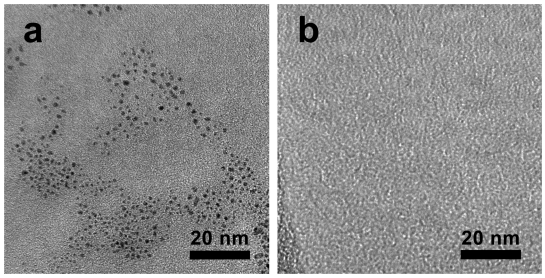


**Figure 4.** (a) $IrO_x$ nanoparticles of ∼2 nm diameter synthesized by aerobic basic hydrolysis of $K_2IrCl_6$ at 1.25 mM. (b) A sample of **2** at 2.3 mM Ir electrolyzed for 36 h at 1.45 V vs NHE applied to a TEM grid using the same conditions as in (a), showing no nanoparticles present; no nanoparticles were found anywhere on the grid. Both images were taken using copper TEM grids coated with an ultrathin carbon film (<3 nm) on a lacey carbon support.

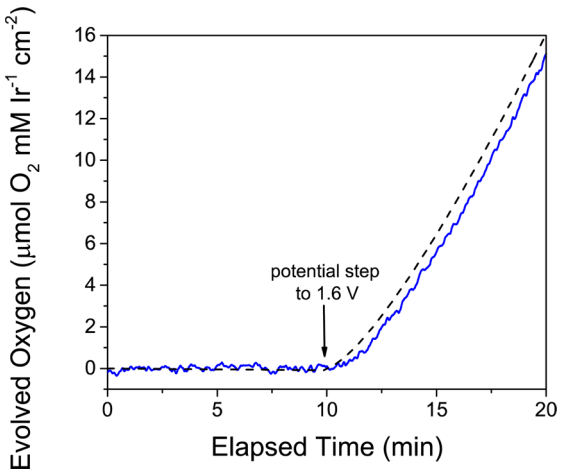


**Figure 5.** Oxygen evolution from a 2 mM solution of **2** after 36 h of bulk electrolysis at 1.45 V in 0.25 M $Na_2SO_4$ (blue, measured by Clark electrode; dashed black, predicted from current passed). A gold electrode was held at 0 V vs NHE for 10 min and then stepped to 1.6 V for 10 min.


dx.doi.org/10.1021/ja5068299 | J. Am. Chem. Soc. 2014, 136, 13826−13834

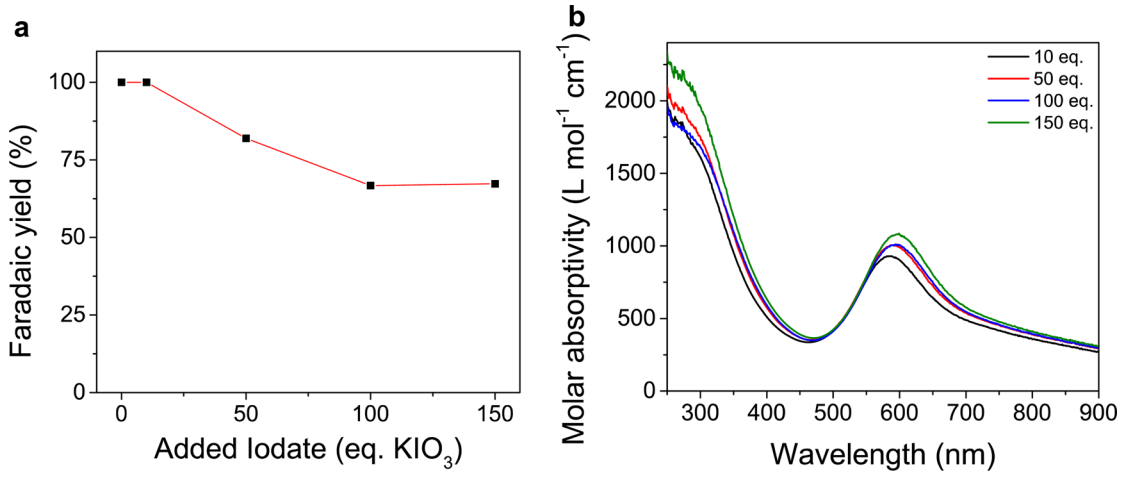


**Figure 6.** Effect of added $KIO_3$ on the Faradaic yield of water oxidation (pH 1.9, 1.6 V vs NHE) with electroactivated **2** (a) and on UV−visible absorbance (b).

potential required to evolve oxygen was pH-dependent as expected, and raising the pH from 1.9 to 2.9 led to observable $O_2$ evolution at an applied potential of 1.40 V (Figure S21a).

In addition, the yield of $O_2$ from the electrosynthesized species was significantly higher than chemically synthesized **4** at the same conditions. Because the effective rate of $O_2$ evolution of electrosynthesized **4** is nearly 3 times higher than the effective rate of $NaIO_4$-synthesized **4** at the applied overpotential of 490 mV, the overall oxygen yield increased about 3-fold (cf. Figures 2 and 5). With reference to the CV of $NaIO_4$-synthesized **4** (Figures S4 and S5) and the Pourbaix diagram of $IO_4^-$,[46,56] we suspected that this could be due to competitive oxidation of residual iodine species rather than water by iridium. Indeed, addition of various amounts of $KIO_3$ to the electrosynthesized blue species and repeating the measurement supported this hypothesis (Figure 6a). At 0−10 equiv, the Faradaic yield remained close to 100%. Increasing the quantity of $IO_3^-$ to 50, 100, and 150 equiv caused a steady reduction in the Faradaic yield, leveling off around 66%, very similar to what was seen with **4** pre-synthesized with $NaIO_4$. The UV−visible spectrum also shifted slightly with increasing amounts of $IO_3^-$, causing a red shift of $\lambda_{max}$ of up to 22 nm at higher concentrations as well as increased absorbance in the UV range that is characteristic of the $I_2/I^-/I_3^-$ equilibrium in aqueous solution[60,64] (Figure 6b). CVs of the electrolyzed blue solution with $KIO_3$ added show new features that are consistent with the CV features of **4** made by $NaIO_4$ (Figure S19). This is strong evidence that the same active species is formed by both chemical and electrochemical oxidation of **2**, and that differences in properties and catalytic performance between the two solutions arise primarily from iodine-based contaminants present after $NaIO_4$ activation.

Previous studies have shown that the choice of the chelate ligand in the precursor strongly affects the rate of $O_2$ evolution with $NaIO_4$.[12,20,30] If similar molecular species are formed after electro-activation, this would suggest that ligand effects would also be prominent in electrode-driven $O_2$ evolution. Therefore, an analogous set of experiments to those performed on **2** was carried out for **3**. The species resulting from activation of **3** with 100 equiv of $NaIO_4$ appeared to be significantly less stable than that from **2**, however. Within 3 h of $NaIO_4$ addition to **3**, the blue color began to fade, and the catalyst solution became a pale green color within 6 h. This is likely due to partial reduction under ambient conditions of the blue Ir(IV) species to yellow Ir(III) species, as we have seen before for this compound after $NaIO_4$ treatment.[20] The destabilization of the Ir(IV) state is probably a result of the poorer donor nature of the neutral bipyridine ligand compared to the anionic pyalc ligand. Because activation, purging with $N_2$, and stirring in air to achieve ambient oxygen levels in the activated solution took some time (see Experimental Section), it was not possible to carry out electrode-driven $O_2$-evolution experiments before the solution derived from **3** had lost a significant amount of its blue color. Experiments that were carried out within 6 h of $NaIO_4$ addition gave an effective rate of 4.45 (±0.13) nmol $O_2$ mM $Ir^{-1}$ $cm^{-2}$ $s^{-1}$ at pH 1.9, about half that observed for the pyalc ligand (Figure 7). In addition, the Faradaic efficiency of activated **3** was only 45% (±5%) at an applied potential of 1.6 V vs NHE (Figure S23), possibly due to an additional step needed for some reduced Ir(III) species to be reoxidized to Ir(IV) in order to enter the catalytic cycle. It is also possible

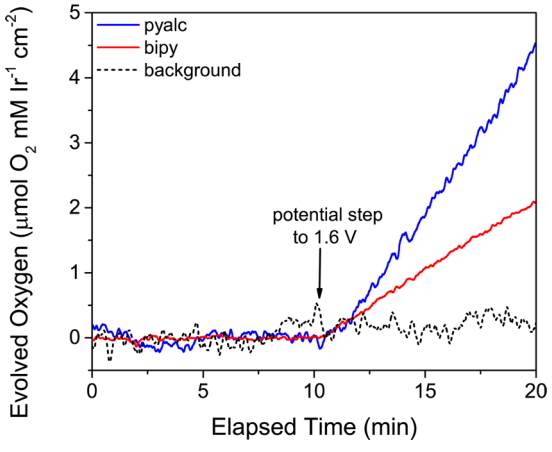


**Figure 7.** Oxygen evolution over time in response to applied potential at a gold electrode for **2** activated with 100 equiv of $NaIO_4$ (pyalc, solid blue) and **3** activated with 100 equiv of $NaIO_4$ (bipy, solid red), showing the difference in rate that results from the different chelate ligand. A control measurement of 0.1 M $KIO_3$ is also shown (dashed black). In addition to their differing rates of $O_2$ evolution (pyalc, 8.5 nmol $O_2$ mM $Ir^{-1}$ $cm^{-2}$ $s^{-1}$; bipy, 4.5 nmol $O_2$ mM $Ir^{-1}$ $cm^{-2}$ $s^{-1}$), they also have different Faradaic yields (pyalc, 59%; bipy, 45%).


dx.doi.org/10.1021/ja5068299 | J. Am. Chem. Soc. 2014, 136, 13826−13834

that some of the current at this potential arises from oxidation of the bipyridine ligand, though bipyridine oxidation is expected to be slow at the acidic pH used for this study.

In addition to the different electrochemical behavior of **3** compared to **2** after activation with excess $NaIO_4$, precursor **3** also showed very different behavior from **2** in electrochemical activation. Higher potential (1.55 V) was required to achieve the characteristic blue color, again probably a result of the poorer donor ability of the neutral bipy ligand. As seen with $NaIO_4$, the solution derived from electrolysis of 1 mM **3** lacked the stability of the solution derived from **2**, decaying to a colorless solution within 3 days of electrolysis. Increasing the concentration to 2 mM and carrying out 36 h of electrolysis of **3** at 1.55 V, furthermore, yielded a deep purple solution with a dark precipitate. We suspect that this results from the relative instability of the bipyridine ligand under highly oxidizing conditions. Synthesis of colloidal IrOx requires an initial iridium concentration >2 mM, and it is likely that less-stable Cp*Ir precursors like **3** are prone to rapid particle formation at concentrations in excess of 2 mM. By contrast, **2** did not show particle formation even at 2.3 mM. These clear differences from the species derived from **2** indicate that the choice of chelate ligand has a significant impact on the stability and catalytic properties of the activated species. Together with the previously mentioned oxidative instability of the bipyridine ligand, **2** seems to be a clearly superior precatalyst for water oxidation compared to **3**, consistent with our previous reports that the pyalc ligand assists in providing greater stability and higher activity than bpy for iridium-based WOCs. These findings are exciting in that they offer a guideline for molecular tuning of these highly promising water-oxidation electrocatalysts.

## ■ CONCLUSION

We present evidence for homogeneous electrocatalysis of water oxidation effectively mediated by preactivated Cp*Ir precatalysts bearing oxidatively stable chelate ligands. The complexes, once activated by Cp* loss using an excess of $NaIO_4$, evolve $O_2$ with minimal lag phase at electrode surfaces when oxidizing potentials are applied, whereas the precursor complexes before activation with $NaIO_4$ do not evolve any $O_2$ under the same conditions. Activation of the complexes is also possible using bulk electrolysis at oxidizing potentials ≥1.4 V vs NHE, and the product of the activation process appears to be very similar regardless of the oxidative activation method used. The electrochemically activated species is a highly active homogeneous catalyst with a low overpotential of 345 mV and high effective rate of $O_2$ evolution. The identity of the chelate ligand has been shown to play a decisive role in the $O_2$-evolution activity of the activated catalyst as well as the stability of its Ir(IV) state. We emphasize the importance of following real time product detection along with current flow through the working electrode, as in this example we have seen that current observed for precursor species bearing the Cp* ligand does not correspond to $O_2$ evolution, but likely stems from oxidation of the sacrificial placeholder ligand Cp*. The reported findings will allow the use the activated species in electrocatalytic applications, with possible extension to integrated photoelectrocatalytic cells such as are often considered for direct solar fuel generation.

## ■ EXPERIMENTAL SECTION

**General Procedures.** High-purity Milli-Q water was used in all experiments. $KNO_3$, $K_2IrCl_6$, and $Na_2SO_4$ (≥99% purity) were purchased from Sigma-Aldrich and used as received. $NaIO_4$ and $KIO_3$ were purchased from Acros Organics and used as received.

**Synthesis of [($\eta^5$-Pentamethylcyclopentadienyl)Ir(2-(2′-pyridyl)-2-propanolate-$\kappa^2$-O,N)OH].** This compound was prepared similarly to our previously reported procedure.[20] Solid 2-(2′-pyridyl)-2-propanol (82 mg, 0.6 mmol) was added under nitrogen to a freshly prepared solution of [($\eta^5$-pentamethylcyclopentadienyl)$_2$Ir$_2$($\mu$-OH)$_3$]OH (0.3 mmol in 20 mL water) and the reaction mixture stirred at room temperature for 16 h. The resulting bright yellow solution was concentrated under reduced pressure to a volume of ca. 0.5 mL and then dried under a nitrogen flow. Further drying under high vacuum yielded compound **2** as a fine yellow powder (258 mg, 90%), which was stored under argon.

**Synthesis of Colloidal Iridium Oxide Solutions.** The procedure was carried out according to Murray and co-workers.[25] 2.5 mM $K_2IrCl_6$ was dissolved in water in a round-bottom flask, then brought to pH 13 with 25% w/v NaOH and immersed in a 90 °C water bath with stirring for 20 min. During this period color changes of the iridium solution were observed from deep reddish-brown to pale green to pale blue and finally to a pale purple color. After 20 min had elapsed, the solution was allowed to cool to room temperature on the benchtop and aged for 24 h before TEM and DLS measurements were taken. We also took an aliquot of this solution immediately following hydrolysis, placed it on ice, and added concentrated HCl to achieve a pH of 1 in order to synthesize a species similar to that reported by Mallouk and co-workers.[26]

**Electrochemical Studies.** Electrochemical experiments were all performed using standard three-electrode measurements carried out on a Princeton Applied Research VersaSTAT-4 or a CH Instruments CHI1200B potentiostat. All potentials were measured against Ag/AgCl reference electrodes (+0.197 V vs NHE) purchased from Bioanalytical Systems, Inc. Working electrodes used were either glassy carbon, gold, or platinum electrodes purchased from Bioanalytical Systems, Inc. (0.017 cm$^2$ surface area) or house-made[65] basal plane graphite electrodes (0.096 cm$^2$ surface area). Counter electrodes were platinum wires (for cyclic voltammetry) or platinum mesh (for controlled-potential electrolysis). Before use, carbon electrodes were thoroughly polished with alumina paste and rinsed extensively with Milli-Q water; gold and platinum electrodes were polished thoroughly with 0.5 $\mu$m diamond paste, then cycled in 0.5 M sulfuric acid over a potential range of −0.375 to 1.8 V vs Ag/AgCl. Controlled-potential electrolyses for $O_2$-evolution studies were carried out in a custom water-jacketed glass cell temperature controlled at 25 °C, with the counter electrode separated from the working and reference electrodes. Gold was used as the working electrode for these studies to minimize background water oxidation relative to platinum and to avoid oxidative damage that carbon would undergo at the potentials and duration required for $O_2$ evolution. Platinum was also used in control experiments to verify the validity of results obtained with gold and to calibrate the oxygen collection efficiency of the electrochemical cell to ensure accurate calculations of Faradaic efficiency. Iridium complex solutions used for cyclic voltammetry and controlled-potential electrolysis were 1−2 mM in iridium and 0.1−0.2 M in electrolyte, where the electrolyte used was $KNO_3$ or $KIO_3$. Iridium solutions were filtered through 0.2-$\mu$m filters of the same type used to filter DLS solutions to ensure that the solutions used for $O_2$ evolution were rigorously comparable to solutions used for DLS. Bulk electrolysis was carried out using the commercially available bulk electrolysis cell from Bioanalytical Systems, Inc. with a platinum gauze working electrode, Ag/AgCl reference electrode, and platinum mesh counter electrode contained in a separate fritted chamber. The concentration of iridium complex used for electrolysis was 1−2 mM in 0.25 M $Na_2SO_4$ electrolyte, and the pH was adjusted with $H_2SO_4$ to between 2.4 and 2.9 when electrolysis was initiated. The potential was increased stepwise from 0.5 V to the final voltage (between 1.4 and 1.6 V vs NHE) in 100-mV steps of 30 s each to prevent current overloads. Spectroelectrochemical experiments used the honeycomb cell commercially available from Pine Instruments.

**Oxygen-Evolution Measurements.** Oxygen-evolution data were collected with a YSI 5300A Clark-type electrode using house-written

software that averaged 100,000 data points at a rate of 6 per second. The Clark electrode was immersed into a custom water-jacketed glass cell equipped with fittings for the reference, working and counter electrodes. Baseline measurements of water were obtained in this cell before $O_2$-evolution measurements, and the calibration of voltage reading to concentration of oxygen was made assuming 253 $\mu$M dissolved oxygen at 25 °C.[66] Baseline slope due to consumption of oxygen by the electrode over time (which becomes evident in longer experiments) was corrected using the control measurements. Iridium catalysts pre-activated with $NaIO_4$ were given sufficient time to allow reaction of all equivalents of $IO_4^-$ in solution, purged with nitrogen to expel excess dissolved oxygen remaining from the synthesis, then stirred in air for a minimum of 1 h to re-attain atmospheric dissolved oxygen levels before use in the oxygen assay. Activation and reaction time for **2** was less than for **3**, and solutions of **4** were ready for assay within 3 h of $NaIO_4$ addition. The activation time was significantly greater for **3** because of its slower rate of formation and $O_2$ evolution,[20] and about 6 h was required for activation, purging, and oxygen equilibration.

**UV−Visible Spectroscopy.** A Varian Cary50 UV−visible spectrophotometer was used for all UV−visible measurements using a 1 cm path length quartz cuvette. Baseline measurements were taken on either neat solvent or blank electrolyte solutions.

**Dynamic Light Scattering Measurements.** DLS experiments were conducted using a 532 nm incident laser (Coherent Verdi), at a scattering angle of 90° (ALV5000, ALV-GmbH). Data were collected in intervals of 30 s for all samples continuously for 15 min in a dark room. The scattered light intensity was monitored throughout, as one indication of the presence of particles. On-board correlator cards (ALV-GmbH) provided the scattered light intensity correlation functions $g(\tau)$ at microsecond resolution. When $g(\tau)$ exhibited a clear exponential decay, signifying diffusive motion and, thus, the presence of particles, average particle sizes were obtained by cumulant analysis, by fitting to a second-order exponential decay function. Iridium samples were filtered through 0.2 $\mu$m filters before DLS analysis to remove any large contaminants. Scattering intensity was correlated to concentration using 320 nm silica bead standards (Bangs Laboratories) at a range of dilutions to correlate intensity to concentration.

**Electron Microscopy.** SEM and SEM-EDX data were taken using a Hitachi SU-70 analytical scanning electron microscope, and TEM and TEM-EDX data were taken using a FEI Tecnai Osiris 200 kV transmission electron microscope. Samples were prepared by applying aqueous solutions of iridium compounds onto a TEM grid and ambient drying. Each sample was investigated three times using different types of TEM grids (silicon monoxide, 5−10 nm carbon, and ultrathin carbon on a lacey carbon support; all from Ted Pella) and different preparatory procedures, including sonication or centrifugation, to thoroughly determine whether or not solutions contained nanoparticles.

## ■ ASSOCIATED CONTENT

### Ⓢ Supporting Information

Additional electrochemical data, UV−visible spectra, electron microscopy, DLS, and $O_2$-evolution data. This material is available free of charge via the Internet at http://pubs.acs.org.

## ■ AUTHOR INFORMATION


### Corresponding Authors

u.hintermair@bath.ac.uk
gary.brudvig@yale.edu


### Notes

The authors declare no competing financial interest.

## ■ ACKNOWLEDGMENTS

This work was partially supported as part of the Argonne-Northwestern Solar Energy Research (ANSER) Center, an Energy Frontier Research Center funded by the U.S. Department of Energy, Number DE-SC0001059 (J.M.T., R.H.C., and G.W.B.), as well as the National Science Foundation via a Graduate Research Fellowship and NSF MRSEC DMR 1119826 (S.W.S.). J.C. acknowledges a catalysis grant from the Division of Chemical Sciences, Geosciences, and Biosciences, Office of Basic Energy Sciences of the U.S. Department of Energy through Grant DE-FG02-84ER13297. U.H. acknowledges support from the Alexander von Humboldt Foundation through a Feodor Lynen Research Fellowship and from the Centre for Sustainable Chemical Technologies at the University of Bath through a Whorrod Research Fellowship. We thank Drs. Alec C. Durrell and Karin J. Young for helpful discussions and Dr. James D. Blakemore for reading of the manuscript. J.M.T. thanks Daryl Smith for fabrication of custom glassware and Rosario Bernardo for machined parts.

## ■ REFERENCES


(1) Lewis, N. S.; Nocera, D. G. *Proc. Natl. Acad. Sci. U.S.A.* **2006**, *103*, 15729.
(2) Blankenship, R. E.; Tiede, D. M.; Barber, J.; Brudvig, G. W.; Fleming, G.; Ghirardi, M.; Gunner, M. R.; Junge, W.; Kramer, D. M.; Melis, A.; Moore, T. A.; Moser, C. C.; Nocera, D. G.; Nozik, A. J.; Ort, D. R.; Parson, W. W.; Prince, R. C.; Sayre, R. T. *Science* **2011**, *332*, 805.
(3) Meyer, T. J. *Acc. Chem. Res.* **1989**, *22*, 163.
(4) Alstrum-Acevedo, J. H.; Brennaman, M. K.; Meyer, T. J. *Inorg. Chem.* **2005**, *44*, 6802.
(5) Gust, D.; Moore, T. A.; Moore, A. L. *Acc. Chem. Res.* **2009**, *42*, 1890.
(6) Yagi, M.; Kaneko, M. *Chem. Rev.* **2001**, *101*, 21.
(7) Wasylenko, D. J.; Palmer, R. D.; Berlinguette, C. P. *Chem. Commun.* **2013**, *49*, 218.
(8) Yagi, M.; Syouji, A.; Yamada, S.; Komi, M.; Yamazaki, H.; Tajima, S. *Photochem. Photobiol. Sci.* **2009**, *8*, 139.
(9) *Molecular Water-oxidation Catalysis: A Key Topic for New Sustainable Energy Conversion Schemes*; Llobet, A., Ed.; John Wiley & Sons, Ltd.: Chichester, UK, 2014.
(10) Hull, J. F.; Balcells, D.; Blakemore, J. D.; Incarvito, C. D.; Eisenstein, O.; Brudvig, G. W.; Crabtree, R. H. *J. Am. Chem. Soc.* **2009**, *131*, 8730.
(11) Blakemore, J. D.; Schley, N. D.; Balcells, D.; Hull, J. F.; Olack, G. W.; Incarvito, C. D.; Eisenstein, O.; Brudvig, G. W.; Crabtree, R. H. *J. Am. Chem. Soc.* **2010**, *132*, 16017.
(12) Parent, A. R.; Brewster, T. P.; De Wolf, W.; Crabtree, R. H.; Brudvig, G. W. *Inorg. Chem.* **2012**, *51*, 6147.
(13) Hintermair, U.; Hashmi, S. M.; Elimelech, M.; Crabtree, R. H. *J. Am. Chem. Soc.* **2012**, *134*, 9785.
(14) Grotjahn, D. B.; Brown, D. B.; Martin, J. K.; Marelius, D. C.; Abadjian, M.-C.; Tran, H. N.; Kalyuzhny, G.; Vecchio, K. S.; Specht, Z. G.; Cortes-Llamas, S. A.; Miranda-Soto, V.; van Niekerk, C.; Moore, C. E.; Rheingold, A. L. *J. Am. Chem. Soc.* **2011**, *133*, 19024.
(15) Savini, A.; Belanzoni, P.; Bellachioma, G.; Zuccaccia, C.; Zuccaccia, D.; Macchioni, A. *Green Chem.* **2011**, *13*, 3360.
(16) Zuccaccia, C.; Bellachioma, G.; Bolaño, S.; Rocchigiani, L.; Savini, A.; Macchioni, A. *Eur. J. Inorg. Chem.* **2012**, *2012*, 1462.
(17) Wang, C.; Wang, J.-L.; Lin, W. *J. Am. Chem. Soc.* **2012**, *134*, 19895.
(18) Park-Gehrke, L. S.; Freudenthal, J.; Kaminsky, W.; DiPasquale, A. G.; Mayer, J. M. *Dalton Trans.* **2009**, 1972.
(19) Ingram, A. J.; Wolk, A. B.; Flender, C.; Zhang, J.; Johnson, C. J.; Hintermair, U.; Crabtree, R. H.; Johnson, M. A.; Zare, R. N. *Inorg. Chem.* **2014**, *53*, 423.
(20) Hintermair, U.; Sheehan, S. W.; Parent, A. R.; Ess, D. H.; Richens, D. T.; Vaccaro, P. H.; Brudvig, G. W.; Crabtree, R. H. *J. Am. Chem. Soc.* **2013**, *135*, 10837.

(21) Harriman, A.; Thomas, J. M.; Millward, G. R. *New J. Chem.* **1987**, *11*, 757.
(22) Castillo-Blum, S. E.; Richens, D. T.; Sykes, A. G. *Chem. Commun.* **1986**, 1120.
(23) Castillo-Blum, S. E.; Richens, D. T.; Sykes, A. G. *Inorg. Chem.* **1989**, *28*, 954.
(24) Nakagawa, T.; Beasley, C. A.; Murray, R. W. *J. Phys. Chem. C* **2009**, *113*, 12958.
(25) Gambardella, A. A.; Bjorge, N. S.; Alspaugh, V. K.; Murray, R. W. *J. Phys. Chem. C* **2011**, *115*, 21659.
(26) Zhao, Y. X.; Hernandez-Pagan, E. A.; Vargas-Barbosa, N. M.; Dysart, J. L.; Mallouk, T. E. *J. Phys. Chem. Lett.* **2011**, *2*, 402.
(27) Hong, D.; Murakami, M.; Yamada, Y.; Fukuzumi, S. *Energy Environ. Sci.* **2012**, *5*, 5708.
(28) Crabtree, R. H. *Chem. Rev.* **2012**, *112*, 1536.
(29) Schley, N. D.; Blakemore, J. D.; Subbaiyan, N. K.; Incarvito, C. D.; D'Souza, F.; Crabtree, R. H.; Brudvig, G. W. *J. Am. Chem. Soc.* **2011**, *133*, 10473.
(30) Codolà, Z.; M S Cardoso, J.; Royo, B.; Costas, M.; Lloret-Fillol, J. *Chem.—Eur. J.* **2013**, *19*, 7203.
(31) Blakemore, J. D., California Institute of Technology, Pasadena, CA, personal communication, 2014.
(32) Young, K. J.; Martini, L. A.; Milot, R. L.; Snoeberger, R. C.; Batista, V. S.; Schmuttenmaer, C. A.; Crabtree, R. H.; Brudvig, G. W. *Coord. Chem. Rev.* **2012**, *256*, 2503.
(33) Hetterscheid, D. G. H.; Reek, J. N. H. *Eur. J. Inorg. Chem.* **2014**, *2014*, 742.
(34) Ikeda-Ohno, A.; Tsushima, S.; Hennig, C.; Yaita, T.; Bernhard, G. *Dalton Trans.* **2012**, *41*, 7190.
(35) Wasylenko, D. J.; Ganesamoorthy, C.; Henderson, M. A.; Berlinguette, C. P. *Inorg. Chem.* **2011**, *50*, 3662.
(36) Bard, A. J.; Faulkner, L. R. *Electrochemical methods: fundamentals and applications*, 2nd ed.; Wiley: New York, 2001.
(37) Barnett, S. M.; Goldberg, K. I.; Mayer, J. M. *Nat. Chem.* **2012**, *4*, 498.
(38) Wang, D.; Groves, J. T. *Proc. Natl. Acad. Sci. U.S.A.* **2013**, *110*, 15579.
(39) Pourbaix, M. *Atlas of electrochemical equilibria in aqueous solutions*; National Association of Corrosion Engineers: Houston, TX, 1974.
(40) Ghosh, P. K.; Brunschwig, B. S.; Chou, M.; Creutz, C.; Sutin, N. *J. Am. Chem. Soc.* **1984**, *106*, 4772.
(41) Liu, F.; Concepcion, J. J.; Jurss, J. W.; Cardolaccia, T.; Templeton, J. L.; Meyer, T. J. *Inorg. Chem.* **2008**, *47*, 1727.
(42) Hurst, J. K. *Coord. Chem. Rev.* **2005**, *249*, 313.
(43) Depasquale, J.; Nieto, I.; Reuther, L. E.; Herbst-Gervasoni, C. J.; Paul, J. J.; Mochalin, V.; Zeller, M.; Thomas, C. M.; Addison, A. W.; Papish, E. T. *Inorg. Chem.* **2013**, *52*, 9175.
(44) Zhang, T.; deKrafft, K. E.; Wang, J.-L.; Wang, C.; Lin, W. *Eur. J. Inorg. Chem.* **2014**, *2014*, 698.
(45) Limburg, B.; Bouwman, E.; Bonnet, S. *Coord. Chem. Rev.* **2012**, *256*, 1451.
(46) Parent, A. R.; Crabtree, R. H.; Brudvig, G. W. *Chem. Soc. Rev.* **2013**, *42*, 2247.
(47) Costentin, C.; Drouet, S.; Robert, M.; Savéant, J.-M. *J. Am. Chem. Soc.* **2012**, *134*, 11235.
(48) Blakemore, J. D.; Schley, N. D.; Olack, G. W.; Incarvito, C. D.; Brudvig, G. W.; Crabtree, R. H. *Chem. Sci.* **2011**, *2*, 94.
(49) Kushner-Lenhoff, M. N.; Blakemore, J. D.; Schley, N. D.; Crabtree, R. H.; Brudvig, G. W. *Dalton Trans.* **2013**, *42*, 3617.
(50) Sheehan, S. W.; Thomsen, J. M.; Hintermair, U.; Crabtree, R. H.; Brudvig, G. W.; Schmuttenmaer, C. A.; submitted.
(51) Fourmond, V.; Jacques, P.-A.; Fontecave, M.; Artero, V. *Inorg. Chem.* **2010**, *49*, 10338.
(52) Zhang, T.; Wang, C.; Liu, S.; Wang, J.-L.; Lin, W. *J. Am. Chem. Soc.* **2013**, *136*, 273.
(53) Tamaki, Y.; Vannucci, A. K.; Dares, C. J.; Binstead, R. A.; Meyer, T. J. *J. Am. Chem. Soc.* **2014**, *136*, 6854.
(54) Hara, M.; Waraksa, C. C.; Lean, J. T.; Lewis, B. A.; Mallouk, T. E. *J. Phys. Chem. A* **2000**, *104*, 5275.
(55) Hoertz, P. G.; Kim, Y.-I.; Youngblood, W. J.; Mallouk, T. E. *J. Phys. Chem. B* **2007**, *111*, 6845.
(56) Ticknor, K. V.; Cho, Y. H. *J. Radioanal. Nucl. Chem.* **1990**, *140*, 75.
(57) Pecht, I.; Luz, Z. *J. Am. Chem. Soc.* **1965**, *87*, 4068.
(58) Connelly, N. G.; Geiger, W. E. *Chem. Rev.* **1996**, *96*, 877.
(59) Turlington, C. R.; White, P. S.; Brookhart, M.; Templeton, J. L. *J. Am. Chem. Soc.* **2014**, *136*, 3981.
(60) Naorem, H.; Devi, S. D. *Spectrochim. Acta Part A, Mol. Biomol. Spectrosc.* **2013**, *101*, 67.
(61) Nakagawa, T.; Bjorge, N. S.; Murray, R. W. *J. Am. Chem. Soc.* **2009**, *131*, 15578.
(62) Lewandowska-Andralojc, A.; Polyansky, D. E.; Wang, C. H.; Wang, W. H.; Himeda, Y.; Fujita, E. *Phys. Chem. Chem. Phys.* **2014**, *16*, 11976.
(63) Note that the classical heterogeneous/homogeneous distinction blurs on the low nanometer scale (i.e., below 2 nm). Dimers such as **4** are expected to have hydrodynamic radii in the order of 13-atom ($3\times d$) to 55-atom ($5\times d$) fcc nanoparticles.
(64) Li, N.; Shi, L.; Wang, X.; Guo, F.; Yan, C. *Int. J. Anal. Chem.* **2011**, *2011*, No. 130102.
(65) Cady, C. W.; Shinopoulos, K. E.; Crabtree, R. H.; Brudvig, G. W. *Dalton Trans.* **2010**, *39*, 3985.
(66) Truesdale, G. A.; Downing, A. L. *Nature* **1954**, *173*, 1236.